Supporting Information

Rational Design of Li_3VO_4@Carbon Core-Shell Nanoparticles as Li-ion Hybrid Supercapacitor Anode Materials

Eunho Lim,[ab] Won-Gwang Lim,[b] Changshin Jo,[b] Jinyoung Chun,[c] Mok-Hwa Kim,[c] Kwang Chul Roh,[c] and Jinwoo Lee*[ab]

[a]Division of Environmental Science and Engineering, Pohang University of Science and Technology (POSTECH), Pohang, Gyeongbuk 37673, Republic of Korea

[b]Department of Chemical Engineering, Pohang University of Science and Technology (POSTECH), Pohang, Gyeongbuk 37673, Republic of Korea

[c]Energy and Environmental Division, Korea Institute of Ceramic Engineering and Technology (KICET), Jinju, Gyeongnam 52851, Republic of Korea

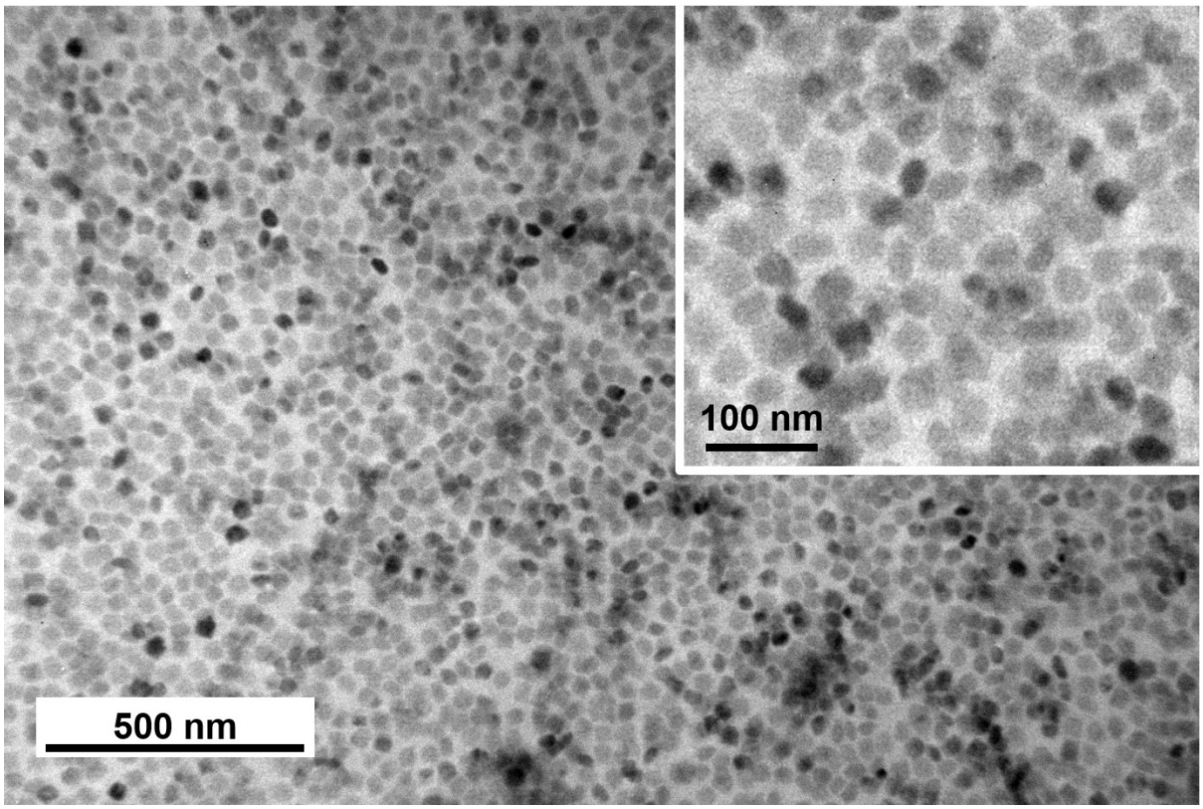

Figure S1. TEM images of as-prepared Li_3VO_4 NPs under different magnification.

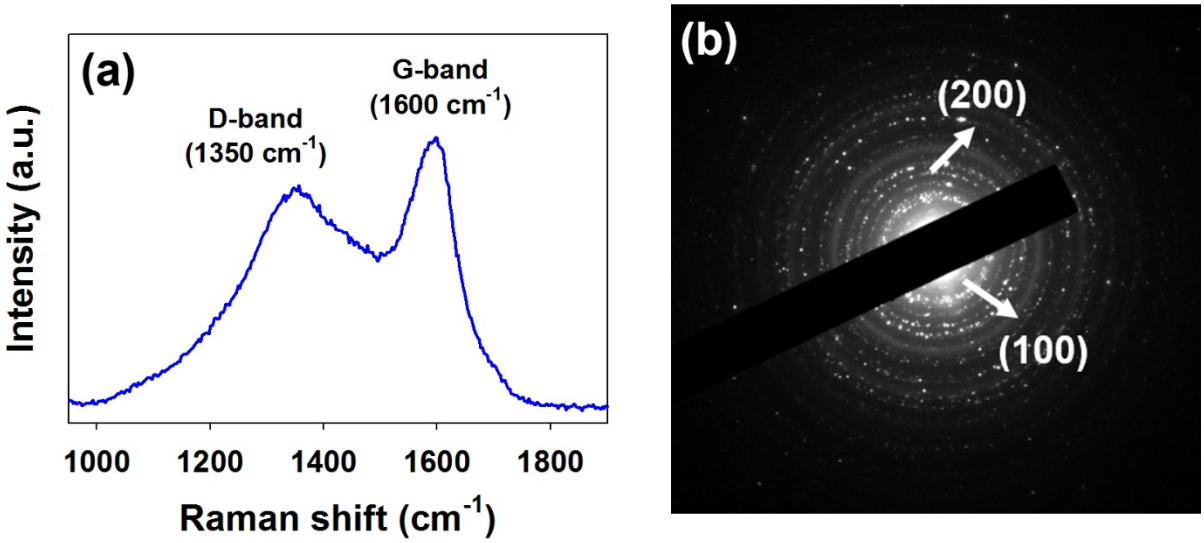

Figure S2. (a) Raman spectrum and (b) SAED pattern of Li_3VO_4@C NPs.

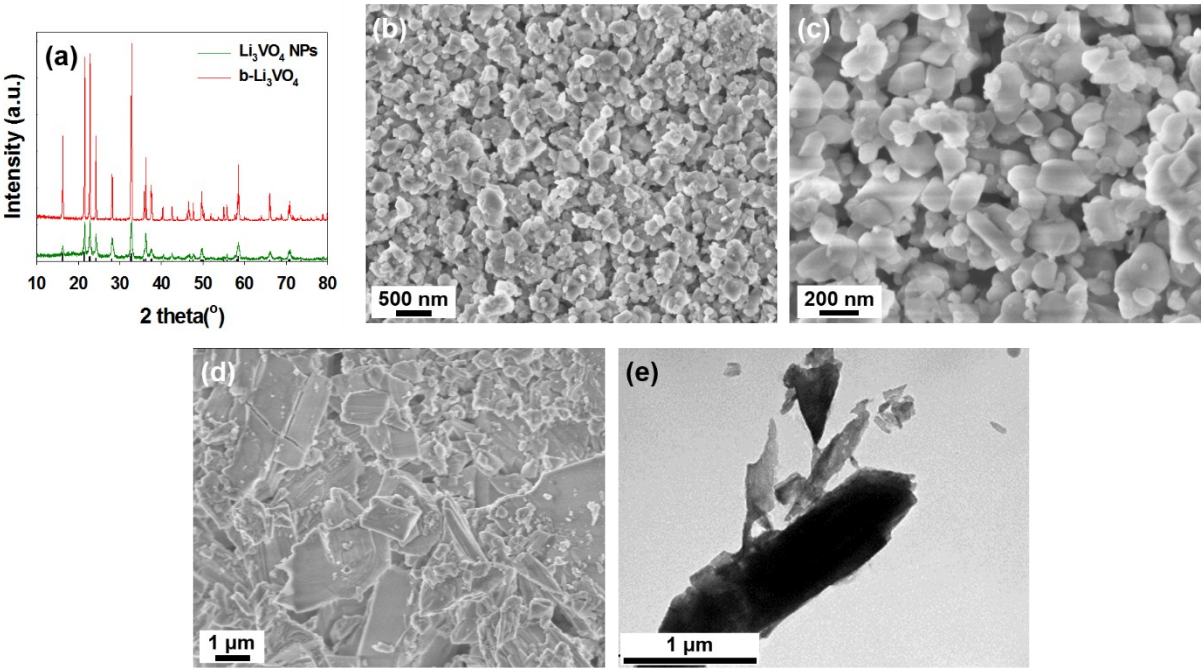

Figure S3. (a) XRD patterns of Li_3VO_4 NPs and b-Li_3VO_4, (b and c) SEM images of Li_3VO_4 NPs, and (d and e) SEM and TEM images of b-Li_3VO_4.

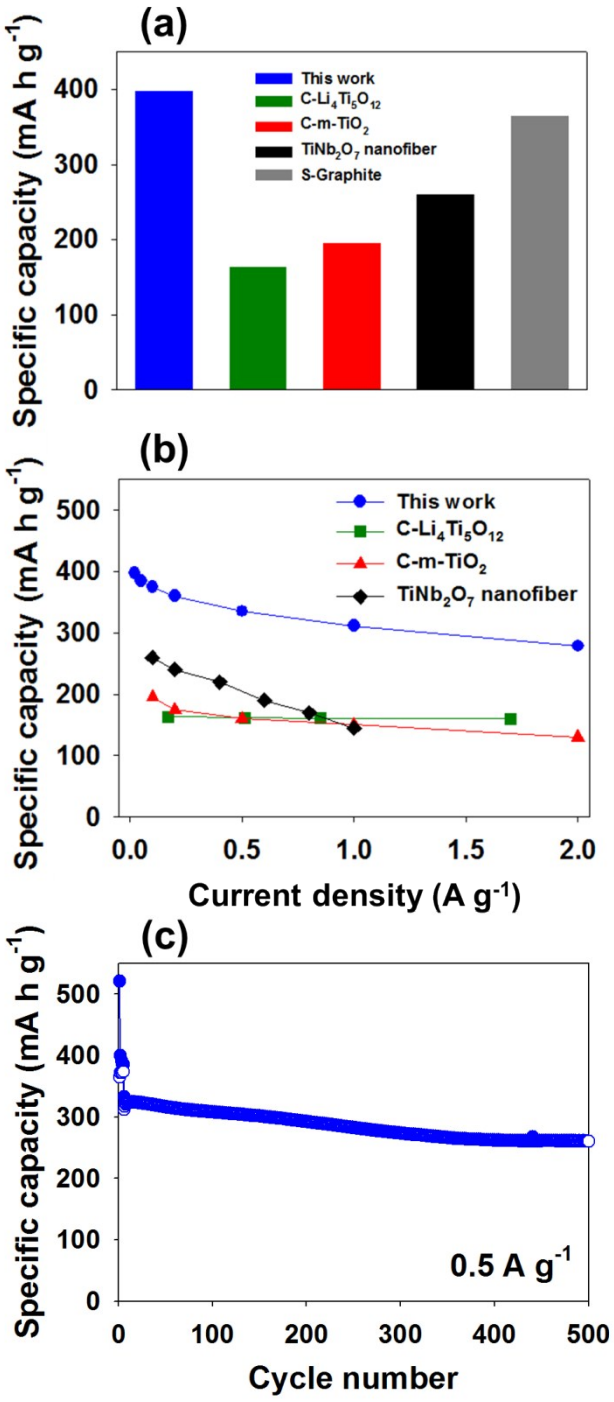

Figure S4. (a) Comparison of capacity on Li_3VO_4@C NPs and results previously reported. (b) Comparison of rate capability on Li_3VO_4@C NPs and results previously reported. (c) Cycle stability of Li_3VO_4@C NPs at 0.5 A g^{-1} in the potential range from 0.2 to 3.0 V (*vs.* Li/Li^+) (Before cycling test, pre-cycling (five cycles) was carried out at 0.02 A g^{-1}).

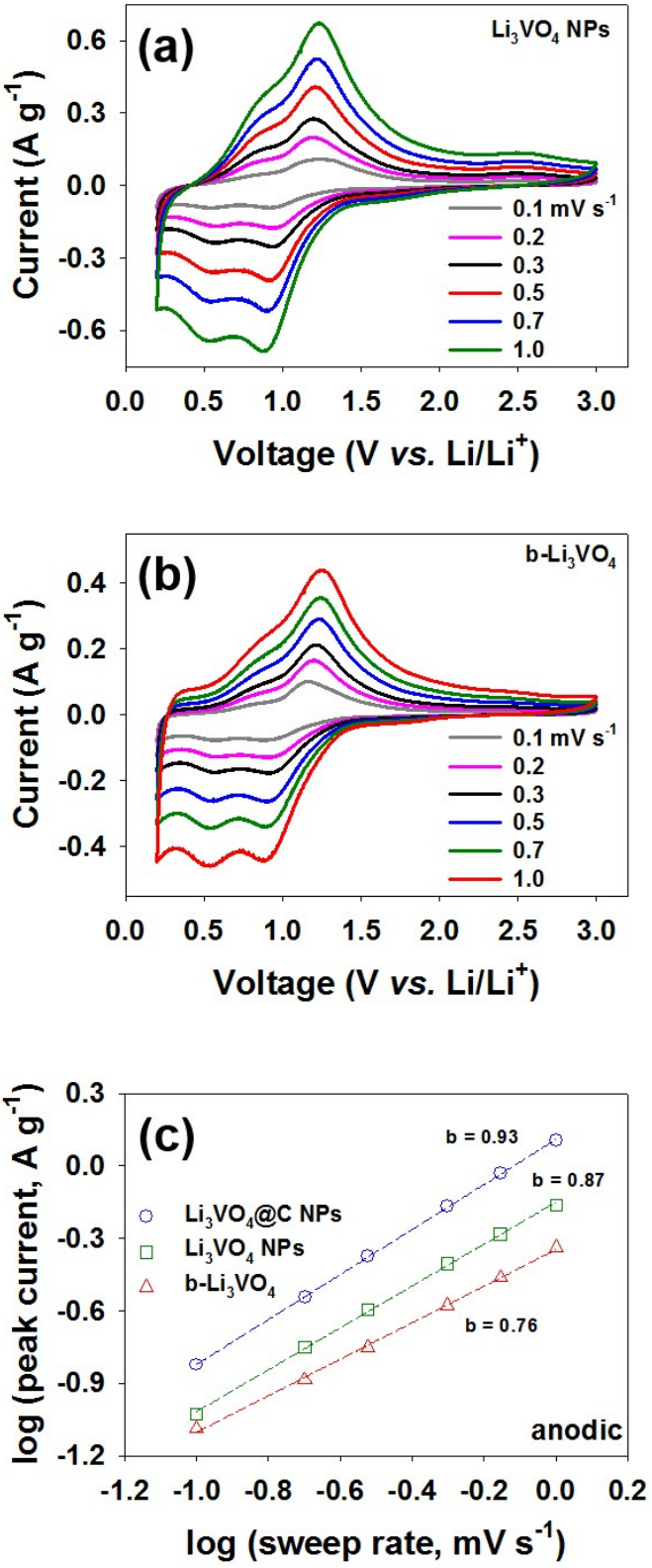

Figure S5. CV curves of (a) Li_3VO_4 NPs and (b) b-Li_3VO_4 at various scan rates from 0.1 to 1.0 mV s^{-1}. (c) *log* (*i*) versus *log* (*v*) plots of anodic current responses on Li_3VO_4 electrodes.

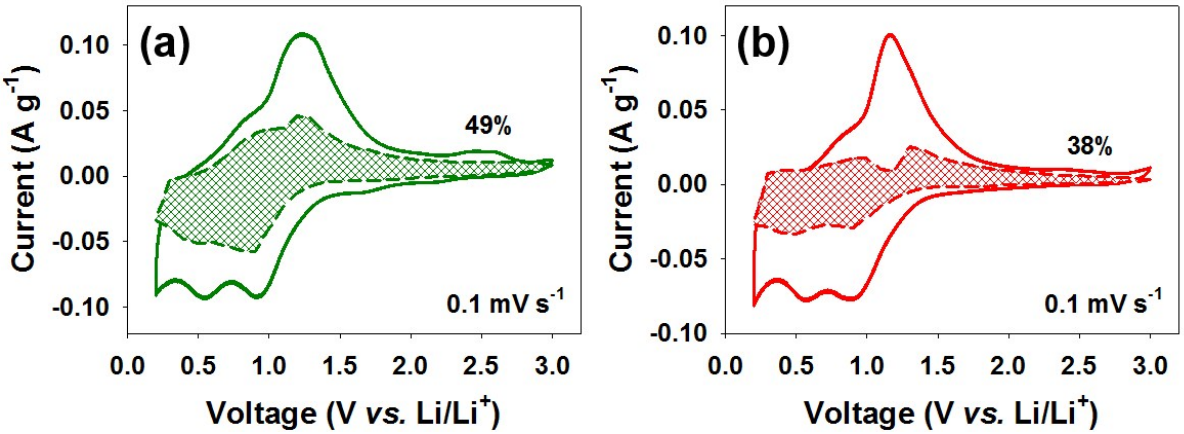

Figure S6. CV curves of (a) Li_3VO_4 NPs and (b) b-Li_3VO_4 with separation between total current (solid line) and pseudocapacitive current (shaded region) at 0.1 mV s^{-1}.

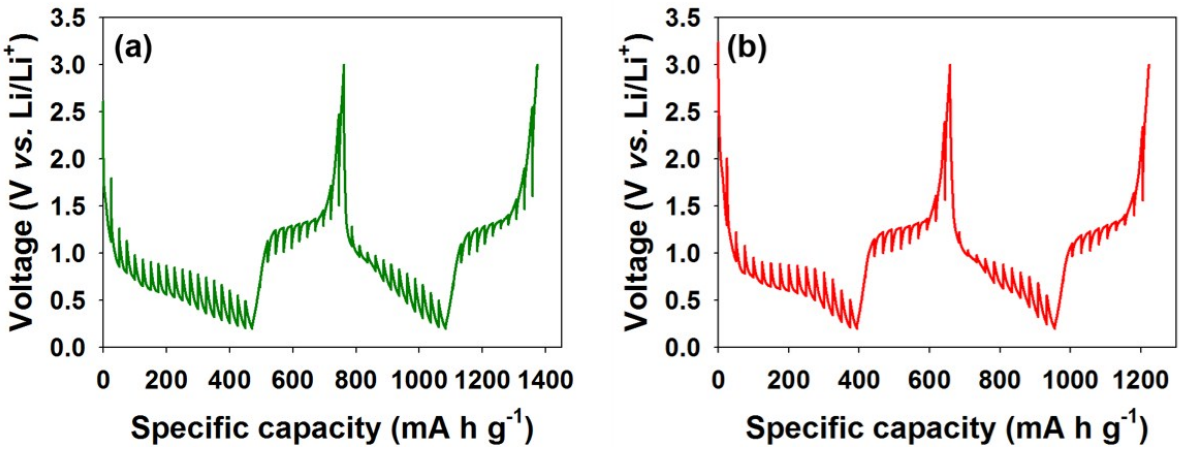

Figure S7. GITT profiles of (a) Li_3VO_4 NPs and (b) b-Li_3VO_4.

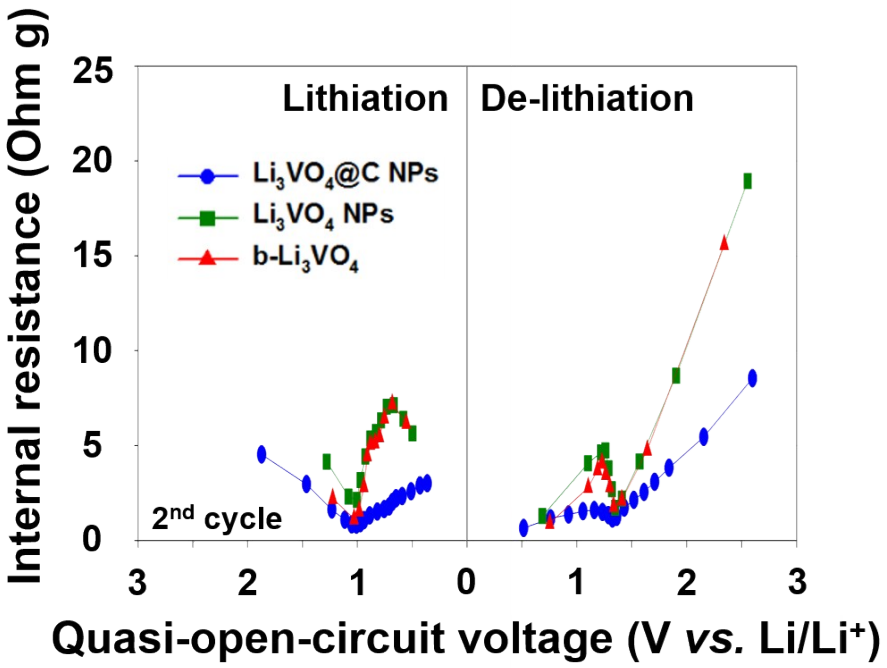

Figure S8. Evolution of internal resistance on Li_3VO_4 electrodes at 2nd cycle.

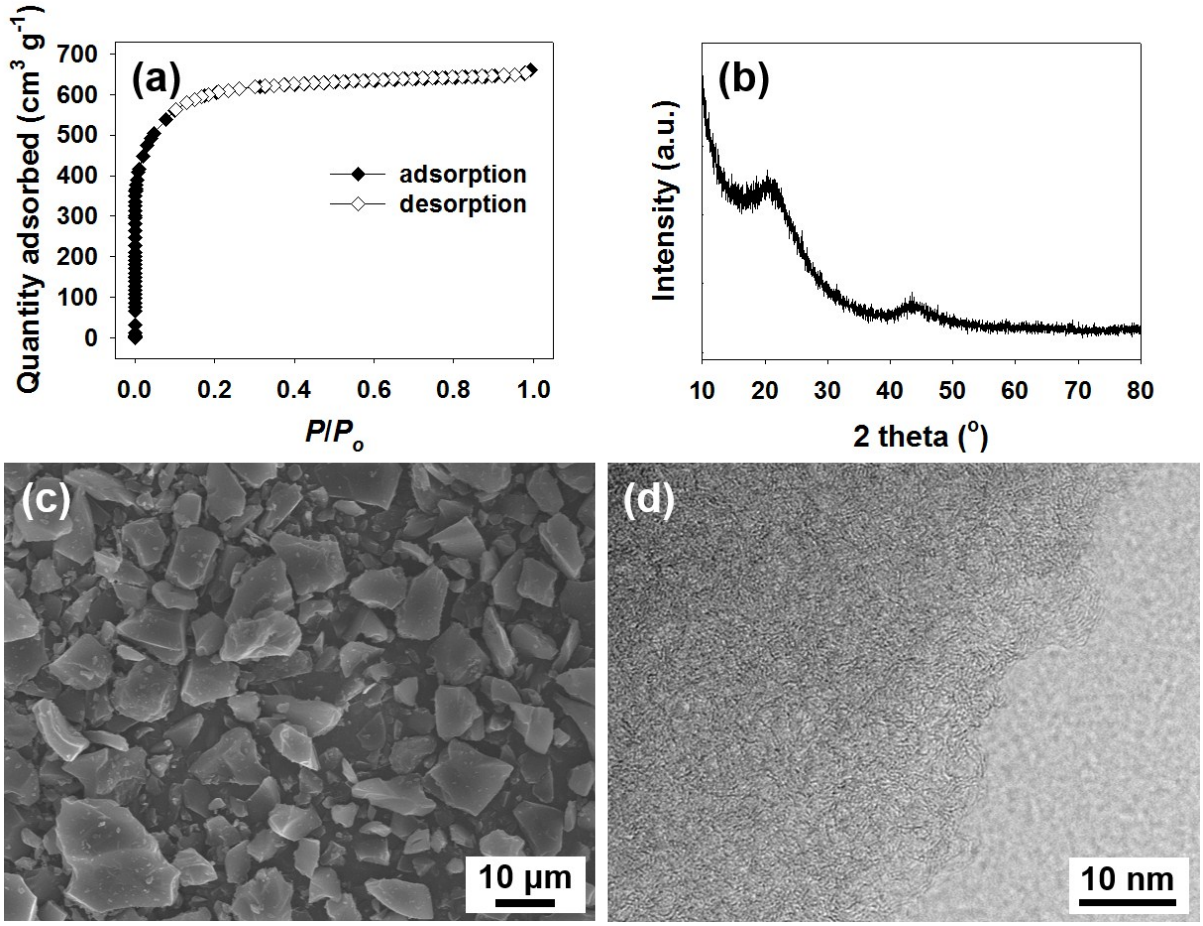

Figure S9. Characterization results of AC: (a) N_2 adsorption and desorption isotherm, (b) XRD pattern, (c) SEM image, and (d) TEM image. The Brunauer-Emmett-Teller (BET) surface area of the AC obtained by N_2 sorption isotherm is 2,274 m^2 g^{-1}. The XRD pattern of AC shows two broad XRD reflection peaks corresponding to the (002) and (101) reflections of graphite carbon, respectively, and demonstrate its amorphous nature. From SEM and TEM images, it is confirmed that the AC has irregular particle shape and disordered micropore structure.

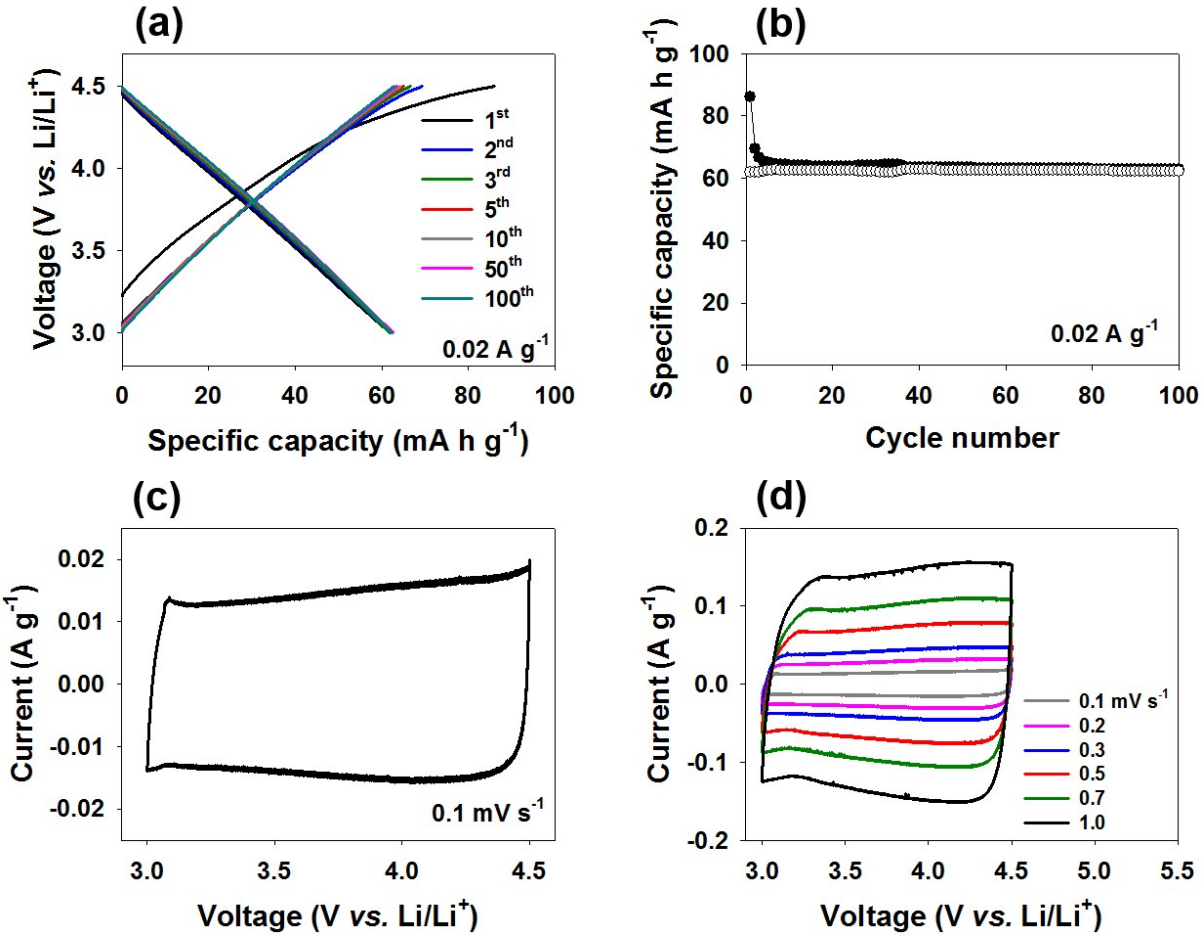

Figure S10. (a) Galvanostatic charge-discharge profiles of AC at 0.02 A g^{-1}. (b) Cycle stability of AC at 0.02 A g^{-1}. (c) CV curve of AC at 0.1 mV s^{-1}. (d) CV curves of AC at various scan rates from 0.1 to 1.0 mV s^{-1}. (a-d) Potential range was 3.0–4.5 V (*vs.* Li/Li^+).

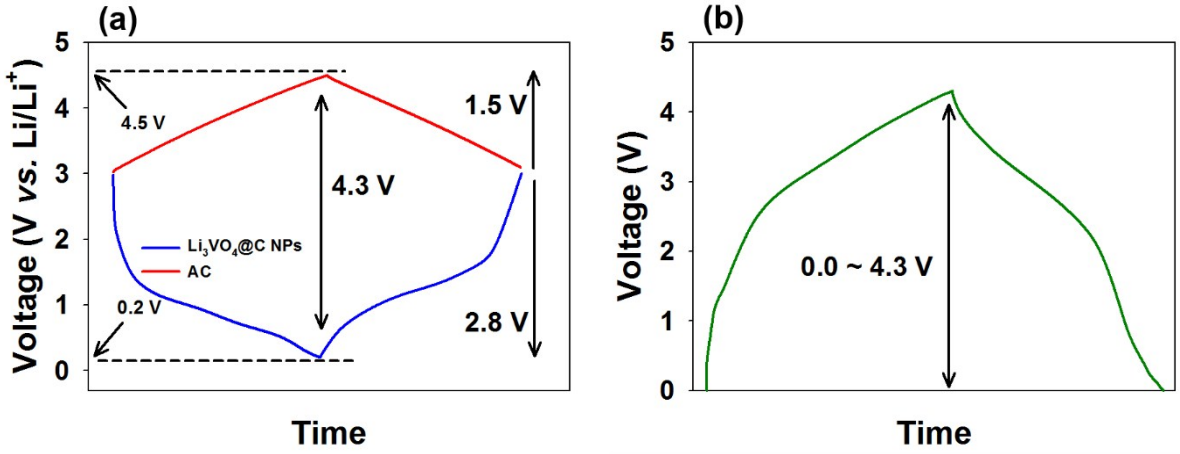

Figure S11. (a) Expected charge-discharge profiles of Li_3VO_4@C NPs (blue solid line) and AC (red solid line) in Li-HSC system. (b) Expected charge-discharge profile of Li-HSC.

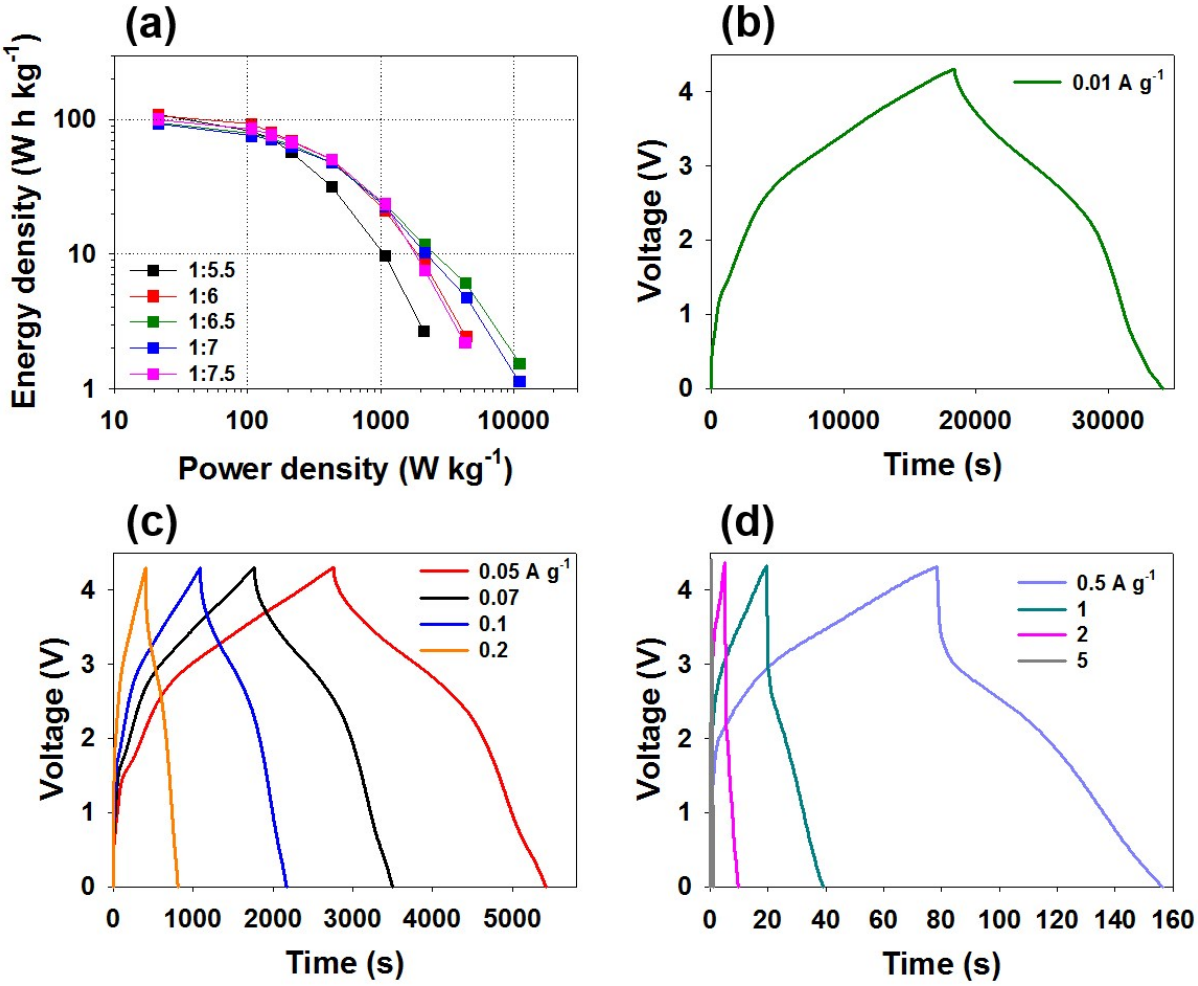

Figure S12. (a) Ragone plots of Li-HSC using Li_3VO_4@C NPs anode and AC cathode with various weight ratio of the anodic and cathodic materials at various current densities from 0.01 to 5 A g^{-1}. (b-d) Galvanostatic charge-discharge profiles of Li-HSC at various current densities from 0.01 to 5 A g^{-1}. (a-d) Potential range was 0.0–4.3 V.

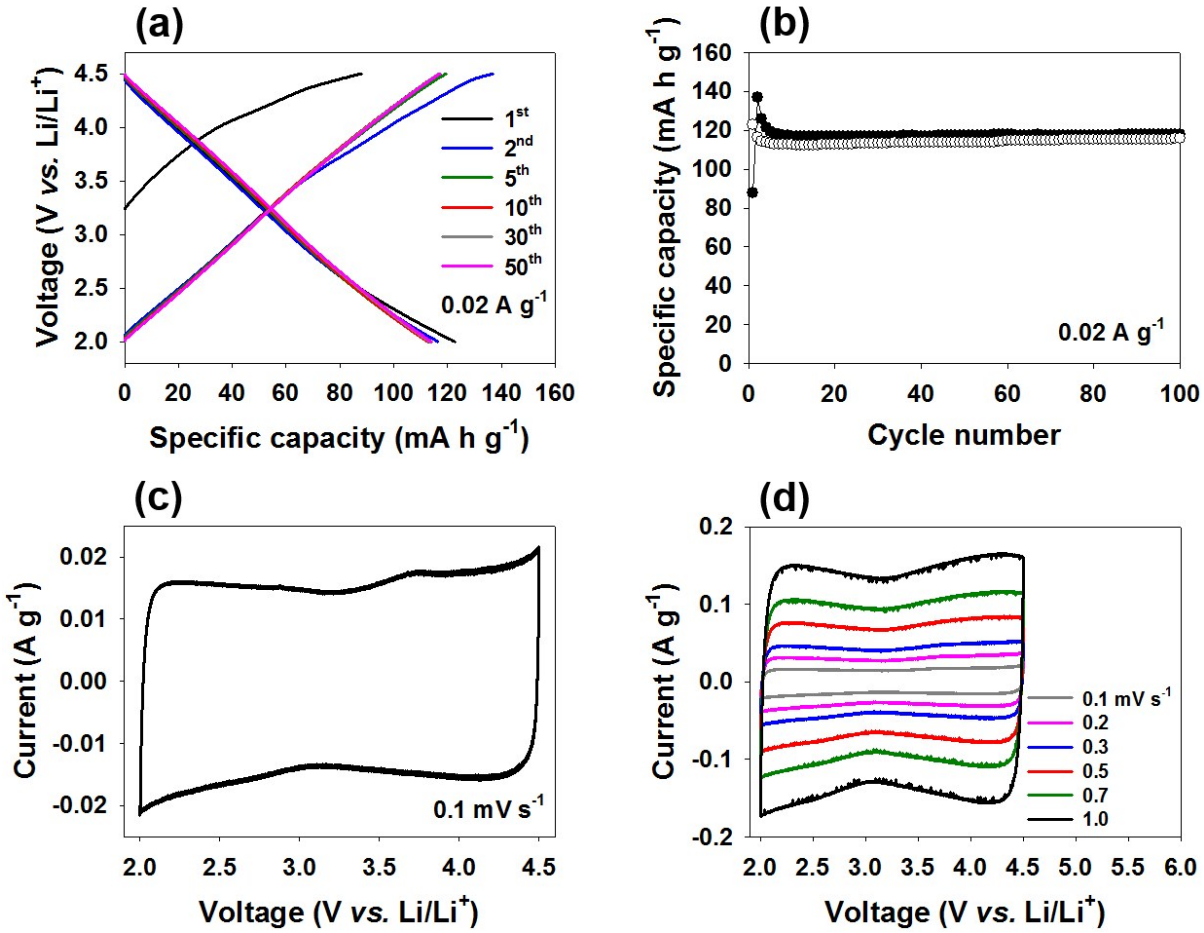

Figure S13. (a) Galvanostatic charge-discharge profiles of AC at 0.02 A g^{-1}. (b) Cycle stability of AC at 0.02 A g^{-1}. (c) CV curve of AC at 0.1 mV s^{-1}. (d) CV curves of AC at various scan rates from 0.1 to 1.0 mV s^{-1}. (a-d) Potential range was 2.0–4.5 V (*vs.* Li/Li^+).

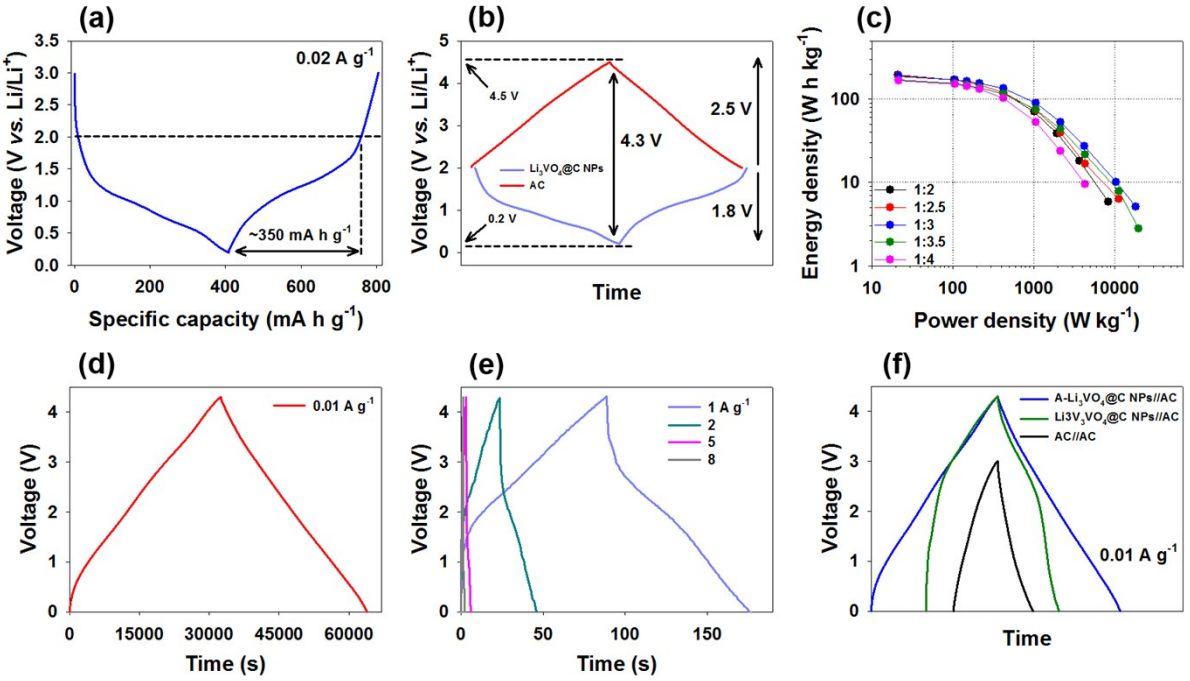

Figure S14. (a) Galvanostatic charge-discharge profile of Li_3VO_4@C NPs at 0.02 A g^{-1}. (b) Expected charge-discharge profiles of pre-activated Li_3VO_4@C NPs (purple solid line) and pre-activated AC (red solid line) in A-Li-HSC system. (c) Ragone plots of A-Li-HSC using pre-activated Li_3VO_4@C NPs anode and pre-activated AC cathode with various weight ratio of the anodic and cathodic materials at various current densities from 0.01 to 8 A g^{-1}. Galvanostatic charge-discharge profiles of A-Li-HSC at (d) 0.01 A g^{-1} and at (e) various current densities from 1 to 8 A g^{-1}. (f) Comparison of galvanostatic charge-discharge profiles on A-Li-HSC, Li-HSC, and symmetric AC//AC EDLC. (c-e) Potential range of A-Li-HSC was 0.0–4.3 V.

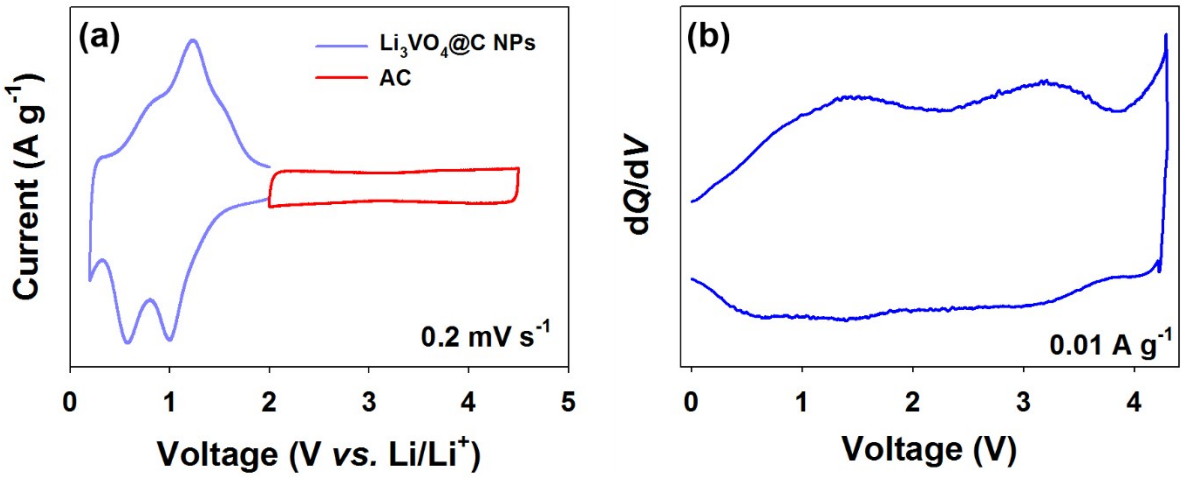

Figure S15. (a) CV curves of Li_3VO_4@C NPs and AC at 0.2 mV s^{-1}. (b) dQ/dV plot obtained from galvanostatic charge-discharge profile of A-Li-HSC at 0.01 A g^{-1}.

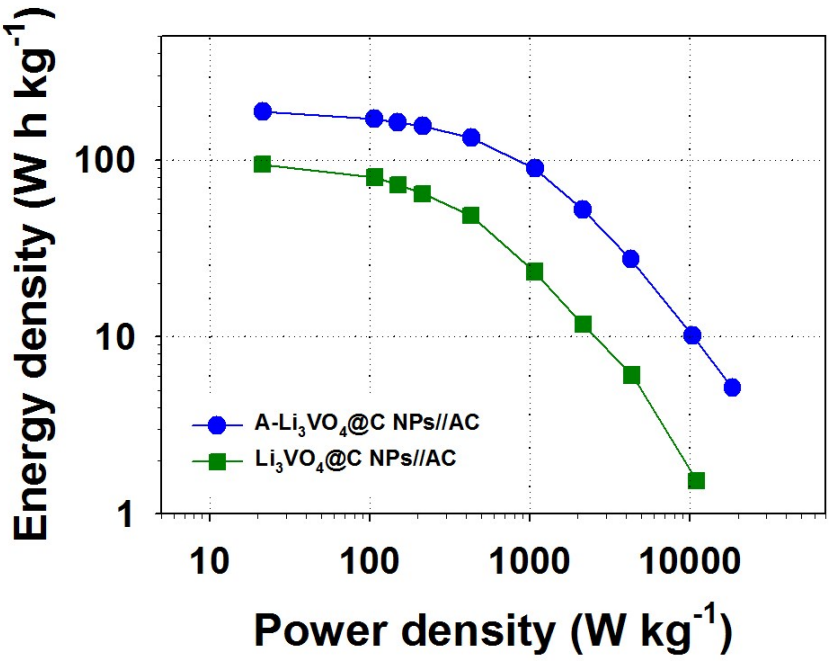

Figure S16. Ragone plots of A-Li-HSC and Li-HSC.

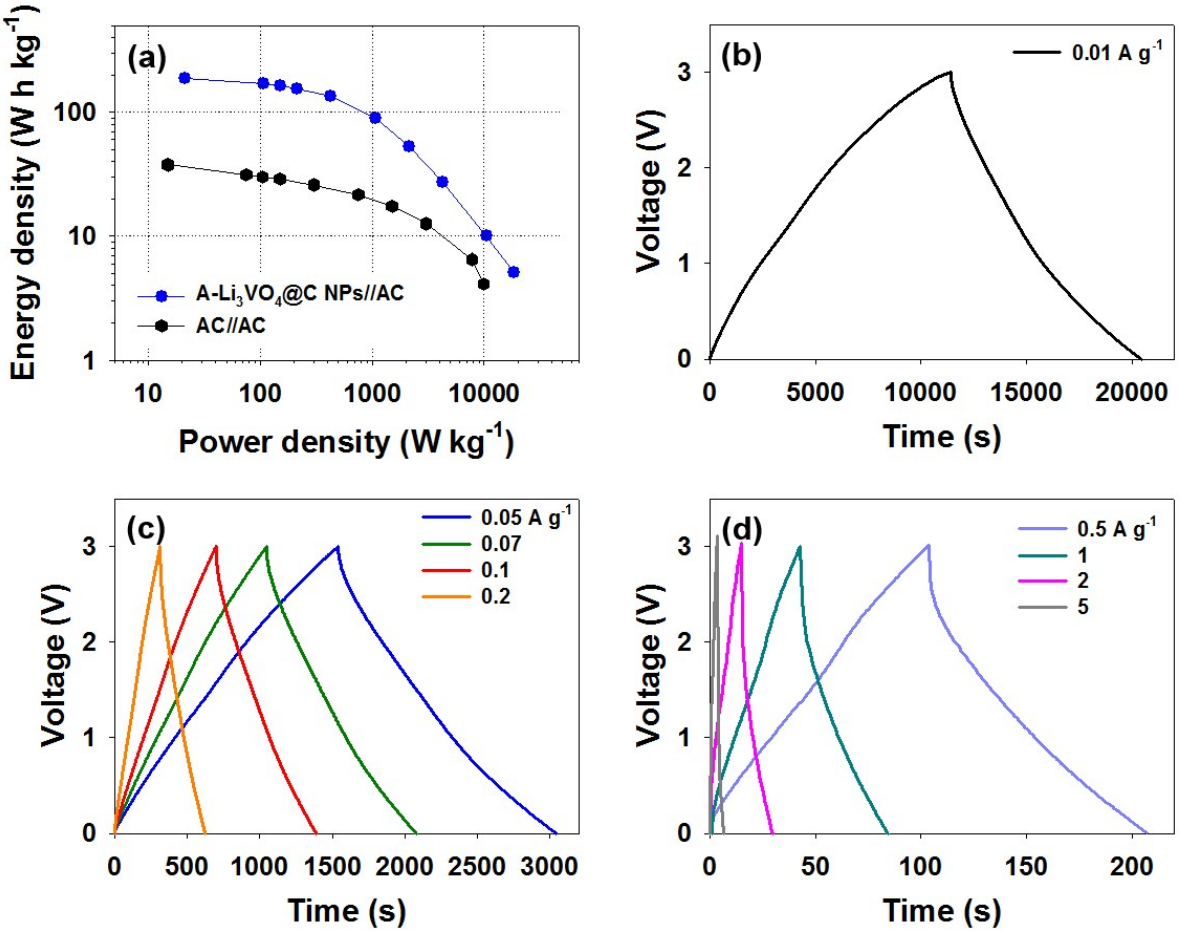

Figure S17. (a) Ragone plots of A-Li-HSC and symmetric AC//AC EDLC. (b-d) Galvanostatic charge-discharge profiles of symmetric AC//AC EDLC at various current densities from 0.01 to 5 A g^{-1}. (a-d) Potential range of symmetric AC//AC EDLC was 0.0–3.0 V.